

Old Dominion University  
**ODU Digital Commons**

---

Physics Faculty Publications

Physics

---

2020

## Collision of $\text{Li}^{2+}$ with $\text{Li}(2s)$ and $\text{Li}(2p)$ : Differential and Total Ionization; Discrete Excitations; Elastic Scattering, and Total Cross Section

H.R.J. Walters

Colm T. Whelan  
*Old Dominion University, [cwhelan@odu.edu](mailto:cwhelan@odu.edu)*

Follow this and additional works at: [https://digitalcommons.odu.edu/physics\\_fac\\_pubs](https://digitalcommons.odu.edu/physics_fac_pubs)

 Part of the [Optics Commons](#)

---

### Original Publication Citation

Walters, H. R. J., & Whelan, C. T. (2020). Collision of  $\text{Li}^{2+}$  with  $\text{Li}(2s)$  and  $\text{Li}(2p)$ : differential and total ionization; discrete excitations; elastic scattering, and total cross section. *Journal of Physics B: Atomic, Molecular, and Optical Physics*, 53(14), 14 pp., Article 145203. <https://doi.org/10.1088/1361-6455/ab89f6>

This Article is brought to you for free and open access by the Physics at ODU Digital Commons. It has been accepted for inclusion in Physics Faculty Publications by an authorized administrator of ODU Digital Commons. For more information, please contact [digitalcommons@odu.edu](mailto:digitalcommons@odu.edu).

# Collision of $\text{Li}^{2+}$ with $\text{Li}(2s)$ and $\text{Li}(2p)$ : differential and total ionization; discrete excitations; elastic scattering, and total cross section

H R J Walters<sup>1</sup>  and Colm T Whelan<sup>2</sup>

<sup>1</sup> Centre for Theoretical Atomic, Molecular, and Optical Physics, School of Mathematics and Physics, Queen's University, Belfast, BT7 1NN, United Kingdom

<sup>2</sup> Department of Physics, Old Dominion University, Norfolk, VA 23529-0116, United States of America

Received 9 January 2020, revised 6 March 2020

Accepted for publication 16 April 2020

Published 17 June 2020



CrossMark

## Abstract

The coupled pseudostate approximation (McGovern *et al* 2009 *Phys. Rev. A* **79** 042707) has been applied to  $\text{Li}^{2+} + \text{Li}(2s, 2p_{0,\pm 1})$  collisions at 16 MeV with emphasis on studying the fully differential ionization measurements of Ghanbari-Adivi *et al* in the azimuthal plane (2017 *J. Phys. B: At. Mol. Opt. Phys.* **50** 215202). The states of the valence electron in the Li target are calculated using the model potential of Stein (1993 *J. Phys. B: At. Mol. Opt. Phys.* **26** 2087). Altogether 164 states with angular momenta  $l = 0$  to 9 are employed in the scattering calculation. It is assumed that the electron in the  $\text{Li}^{2+}$  is frozen in the 1s state and its screening of the  $\text{Li}^{2+}$  nucleus is fully taken into account. Previous calculations on this system (3DW-EIS and CDW-EIS) have treated the  $\text{Li}^{2+}$  as a bare ion with a nuclear charge of 2 au. Except for normalisation, agreement with the experimental data of Ghanbari-Adivi *et al* is generally quite good. But, where agreement is best it is found that the cross section is very much first Born. Except in one case, quite good accord is also obtained with the 3DW-EIS calculations of Ghanbari-Adivi *et al*, particularly on normalisation. Screening by the 1s electron has little effect on the fully differential calculations undertaken here. The double differential cross section  $d^2\sigma/dEdq_t$  and the single differential cross section  $d\sigma/dE$  are also calculated. Here 1s screening is found to be important at large (transverse) momentum transfers  $q_t$  and large ejection energies  $E$ . In addition, the pseudostate approximation gives cross sections for discrete transitions, total ionization and total scattering.

Keywords:  $\hat{\text{L}}\{2+\}$ ,  $\text{Li}(2s)$ ,  $\text{Li}(2p)$ , ionization, discrete excitations, pseudostate approximation

(Some figures may appear in colour only in the online journal)

## 1. Introduction

Cold target recoil ion momentum spectroscopy (COLTRIMS) [1, 2] has been a highly successful technique for the detailed study of differential ionization of atoms and molecules. It is

also known as the reaction microscope (ReMi). One limitation of COLTRIMS has been the mass of the target, which is restricted to light systems such as hydrogen and helium. However, one advantage is that, since the method depends on momentum balance, it can be used in situations where the ionizing projectile is deflected through a very small angle while the momentum transfer is still measurable. Such is usually the case for heavy projectiles like ions. In a very important new development in which a magneto-optical trap (MOT) is introduced into the COLTRIMS set-up, it has now



Original content from this work may be used under the terms of the [Creative Commons Attribution 4.0 licence](https://creativecommons.org/licenses/by/4.0/). Any further distribution of this work must maintain attribution to the author(s) and the title of the work, journal citation and DOI.

become possible to study targets very much heavier than hydrogen or helium. This new approach is named MOTReMi [3, 4] so far, applications have been made to ionization of Li by protons [5],  $O^{8+}$  [5–7], and most recently, by  $Li^{2+}$  [8].

Positive ion projectiles, unlike electrons, enable us to change the strength of the interaction with the target by varying the charge. A useful parameter in this regard is the ratio of the charge of the projectile to its speed (all in atomic units), usually called  $\eta$ . Thus measurements have been made for 6 MeV protons on Li ( $\eta = 0.06$ ), 24 MeV  $O^{8+}$  on Li ( $\eta = 1.03$ ) and now 16 MeV  $Li^{2+}$  on Li ( $\eta = 0.21$ ). The smaller  $\eta$ , the more we expect to be in a perturbative (usually first Born) regime, the larger  $\eta$ , the less effective should perturbation theory be.

But  $\eta$  is a rough parameter. For total ionization cross sections it is probably quite good. But, for differential ionization, it is too crude an object. Here we must expect the viability of perturbation theory to depend upon the particular kinematical arrangement. Thus the first Born approximation does not take account of the interaction between the projectile and target nuclei (suitably screened by any passive electrons if necessary) (we shall refer to this as the NN interaction) and so we must not expect it to be viable in situations where the NN interaction may be important [9–15] (usually the larger momentum transfers). However, for those kinematics which contribute most to the total ionization cross section,  $\eta$  may not be a bad guide.

The most rigorous test of theory is presented by fully differential cross sections (FDCS), in the case of single ionization also called triple differential cross sections (TDCS). Some FDCSs have been measured for  $O^{8+}$  impacting on Li(2s) and Li(2p) at 24 MeV ( $\eta = 1.03$ ) [6, 7].

Lithium is a convenient target for theory since it should be possible to treat it as a one-electron system in the presence of a core of frozen  $1s^2$  electrons. Furthermore, it has been feasible experimentally to excite the ground state 2s electron to the 2p state and so we have the opportunity of studying ionization both from a spherically symmetric ground state and a non-spherically symmetric excited state. The recent appearance of new FDCS measurements for  $Li^{2+}$  on Li(2s, 2p) at 16 MeV ( $\eta = 0.21$ ) [8] extends the rigorous test of theory into a new domain and into a region where perturbation theory has a better chance of being successful. We shall see how this works out.

While FDCSs are the most desirable comparison with theory, lower order differential cross sections, such as double differential (DDCS) and single differential (SDCS) can also be very useful, as can be seen in [9–16]. Indeed, having the complete set of experimental data on differential cross sections, including the total ionization cross section, is to be recommended for checking consistency.

In this paper we apply the powerful method of the coupled pseudostate approximation [9–18] to study the new data on  $Li^{2+} + Li$  FDCSs [8]. This approximation has already been used to study Li(2s) and Li(2p) targets for the cases of p and  $O^{8+}$  projectiles [15]. We shall assume that the electron in the  $Li^{2+}$  is in the 1s state. Note that we do not assume that the  $Li^{2+}$  is a bare ion with nuclear charge  $Z_p = 2$  au, unlike other theoretical calculations [8, 19]. Ghorbani *et al* [19] have

remarked that a proper treatment of the 1s electron in the  $Li^{2+}$  projectile may explain some discrepancies they see between their theory and experiment. Whereas we do not give the 1s electron in  $Li^{2+}$  full rein, the binding energy of this electron is so large that a frozen orbital treatment should give the right indication of its importance, or not. We have previously used this frozen orbital approximation for bound orbitals in  $Au^{24+}$  and  $Au^{53+}$  projectiles [14].

It is useful to highlight the important differences between the present work and the earlier calculations of Ghanbari-Adivi *et al* [8] and Ghorbani *et al* [19] on the  $Li^{2+} + Li$  system. Both these works are based on the same continuum distorted wave philosophy but differ in some details. In both cases, the long-range interaction between the projectile and the bound target electron in the initial state is taken into account by an eikonal phase, while the interaction between the projectile and the ionized electron in the final state is represented by a Coulomb wave in which the ejected target electron scatters off the projectile, assumed to be a bare charge of 2 units; the remaining interactions between the projectile and the target are treated perturbatively. Ghorbani *et al* [19] use the continuum distorted wave eikonal initial state approximation (CDW-EIS) [20, 21] and work within the framework of the impact parameter approximation. On the other hand, Ghanbari-Adivi *et al* [8] adopt a fully quantal treatment, described as the three-body eikonal initial state approximation (3DW-EIS). However, we have shown in [9] that an excellent approximation to a full wave treatment, at all but the lowest impact energies, has the appearance of the impact parameter formalism. To dismiss such an approximation as ‘semiclassical’ on this account is to totally misunderstand the situation. Consequently, we do not consider the difference between the impact parameter treatment of Ghorbani *et al* [19] and the full quantal treatment of Ghanbari-Adivi *et al* [8] to be significant for the situation they have studied, i.e.  $Li^{2+} + Li$  at 16 MeV.

Where differences could arise are on more minor matters such as the choice of target wave functions and the screening of the  $1s^2$  electrons in Li. Here both sets of authors use Hartree–Fock wave functions [22] for the initial state (2s or 2p) of the active target electron. Where they differ is in the representation of the final ionized electron in the field of the target. For this Ghorbani *et al* [19] use a pure Coulomb wave with an effective charge  $Z_{\text{eff}} = n_i \sqrt{-2\epsilon_i}$ , where  $n_i$  and  $\epsilon_i$  are the principal quantum number, and energy, of the initial state of the active target electron. This is intended to take some account of the shielding of the Li nucleus by the  $1s^2$  passive electrons. By contrast, Ghanbari-Adivi *et al* [8] generate the final ionized state by solving the equation for the electron in the static Hartree–Fock field of the target which can be described by an effective charge  $Z_{\text{eff}}(r)$  which varies from  $Z_T$  (the full Li nuclear charge = 3 au) at  $r = 0$  to 1 au as  $r \rightarrow \infty$ , where  $r$  is the distance measured from the Li nucleus. In this way screening of the nucleus by the  $1s^2$  electrons is nicely taken into account.

However, neither of these approaches guarantees that the initial and final states of the active electron are orthogonal (although they may be pretty well close to orthogonality, this

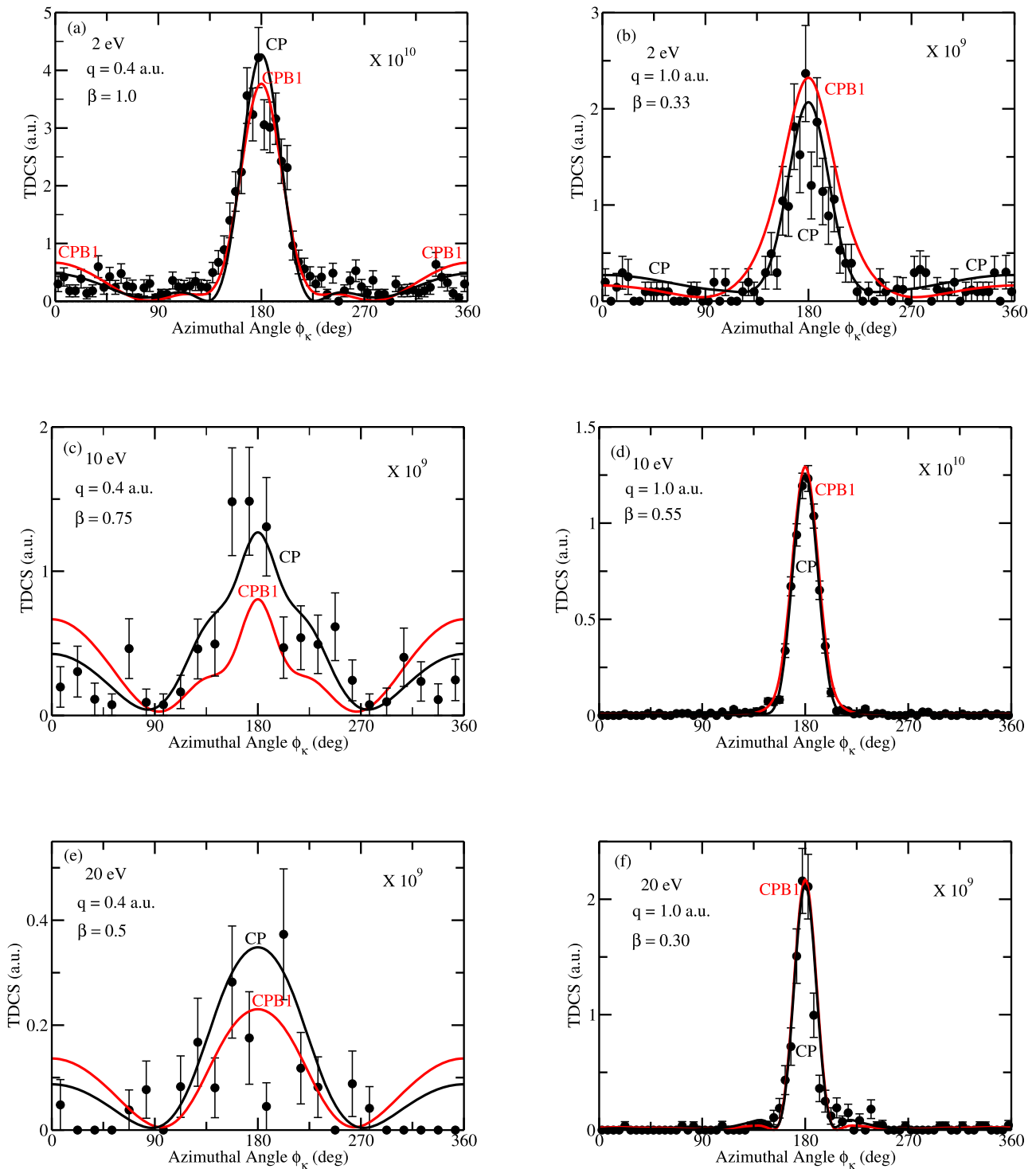


**Figure 1.** TDCS (in the laboratory frame) for 16 MeV  $\text{Li}^{2+}$  impact on  $\text{Li}(2s)$ . The energy of the ejected electron in eV and the momentum transfer  $q$  of the  $\text{Li}^{2+}$  projectile in au are indicated on each panel. Approximations: CP (black curve); CPB1 (red curve). Experimental data from [8] have been normalised as described in text to give best visual fit to CP curve in each case.

remains to be tested). We have pointed out in [23] that this lack of orthogonality can lead, at the first Born level, to spurious  $1/q^4$  behavior of the cross section, rather than  $1/q^2$ , as the momentum transfer  $q$  tends to zero. As the first Born component of the scattering amplitude dominates at small  $q$ , this needs to be kept in mind. Also, as Ghorbani *et al* [19] have shown, use of approximate wave functions can lead to

significant post-prior discrepancy in the CDW-EIS approximation, the extent of the discrepancy depending very much on the kinematics (see figure 1 of Ghorbani *et al* [19]). Ghanbari-Adivi *et al* [8] do not mention post-prior discrepancy in the 3DW-EIS approximation.

In contrast to the continuum distorted wave approximations discussed above, our coupled pseudostate approach is

**Table 1.** Integral cross sections (in units of  $a_0^2$ ) for  $\text{Li}^{2+}$  impact on  $\text{Li}(2s)$  and  $\text{Li}(2p_{0,\pm 1})$  at 16 MeV.

Initial state	Approx.	Li(2s)	Li(2p)	Li(3s)	Li(3p)	Li(3d)	Li(4s)	Li(4p)	Li(4d)	Li(4f)	Other Disc.	Ionization	Total
Li(2s)	CPB1	3.06	22.99	0.32	0.15	0.49	0.066	0.062	0.16	0.015	0.37	2.14	29.45
Li(2s)	CP	2.56	22.37	0.31	0.15	0.50	0.065	0.061	0.16	0.016	0.37	2.12	28.31
Li(2s)	CPBARE	2.47	19.77	0.31	0.15	0.49	0.064	0.059	0.16	0.016	0.36	1.99	25.83
Li(2p <sub>0</sub> )	CPB1	3.01	2.66	1.61	0.35	15.03	0.12	0.074	2.57	0.20	2.28	4.53	32.41
Li(2p <sub>0</sub> )	CP	2.51	2.20	1.23	0.35	14.00	0.11	0.074	2.47	0.20	2.25	4.50	29.87
Li(2p <sub>0</sub> )	CPBARE	2.51	2.11	1.23	0.34	13.96	0.11	0.073	2.44	0.20	2.19	4.39	29.54
Li(2p <sub>±1</sub> )	CPB1	9.99	5.77	4.56	0.96	15.29	0.35	0.21	2.61	0.18	2.58	5.12	47.59
Li(2p <sub>±1</sub> )	CP	8.88	5.17	3.79	0.95	13.13	0.32	0.21	2.40	0.18	2.48	5.05	42.55
Li(2p <sub>±1</sub> )	CPBARE	8.87	5.08	3.79	0.95	13.13	0.32	0.21	2.42	0.18	2.52	4.95	42.43

completely different. Firstly, it is non-perturbative, but does depend upon the quality of the pseudostate basis used; we have reason to believe that the basis is good for present purposes [15]. In principle, the basis takes account of all important dynamical factors, including those associated with the initial and final state interactions of the projectile with the active electron. In particular, it gives a description (dependent upon the basis) of all the main physical processes, e.g. elastic scattering, discrete excitations of the target, total ionization; in this sense we get a complete, and internally consistent, picture of the outcomes of the collision (e.g. see table 1 of the present paper). Of especial relevance to the Li target is the dominant resonance coupling between the Li(2s) and Li(2p) states. This is treated explicitly in the coupled pseudostate approach, unlike the continuum distorted wave approximation. We also take account of the 1s electron in  $\text{Li}^{2+}(1s)$  which in the distorted wave approximations is treated as a bare ion with charge +2 au.

In this work, we also calculate the first Born approximation. This serves three purposes. Firstly, it is a useful standard against which to measure other approximations. Secondly, if it should turn out that we are in the first Born regime, then it is a strong test of the experimental data, unclouded by the correctness, or otherwise, of the more difficult treatment of higher order effects. Thirdly, it is a check on the pseudostate basis and approximation [15]. Since the pseudostate approximation can be run in first Born mode, failure to reproduce the independently calculated first Born limit would reflect badly upon it, e.g. an inadequate pseudostate basis.

We begin in section 2 with a short review of the coupled pseudostate approximation used here, which is described in greater detail in [9–18]. Some calculational details are given in section 3. Results are presented in section 4. Here we make comparison with the recent experimental data of Ghanbari-Adivi *et al* [8], the main motivation for this paper, and with the CDW-EIS and 3DW-EIS approximations of Ghorbani *et al* [19] and Ghanbari-Adivi *et al* [8]. A few significant differences are found, although there is rough overall agreement. Here, we are also interested in how close the results are to a pure first Born approximation. Conclusions are presented in section 5. Throughout we use atomic units (au) in which  $\hbar = m_e = e = 1$ . The symbol  $a_0$  denotes the Bohr radius and all reported differential cross sections refer to the laboratory frame of reference [9].

## 2. Theory

The theory we require here is a combination of that developed in [15] for a bare ion scattering off Li and the treatment described in [14] for dealing with a structured projectile in which the electrons are assumed to be frozen.

As in [15], we use the model potential of Stein [24] for the Li atom:

$$V_A = -V_{\text{core}}^{\text{T}}(r) + V_{\text{exch}}(r) + V_{\text{pol}}^{\text{core}}(r) \quad (1)$$

here  $\mathbf{r}$  is the position vector of the valence electron relative to the nucleus,  $V_{\text{core}}^{\text{T}}$  is the static potential of the  $\text{Li}^+(1s^2)$  core as seen by a unit positive charge,  $V_{\text{exch}}$  represents the exchange interaction between the valence electron and the  $1s^2$  core electrons, and  $V_{\text{pol}}^{\text{core}}$  accounts for polarisation of the  $1s^2$  core by the valence electron. Explicitly,

$$\begin{aligned} V_{\text{core}}^{\text{T}} &= \frac{Z_{\text{T}}}{r} - \frac{1}{2\pi} \int \frac{R_{1s}(r')R_{1s}(r')}{|\mathbf{r} - \mathbf{r}'|} d\mathbf{r}' \\ &= \frac{(Z_{\text{T}} - 2)}{r} + V_{\text{SR}}^{\text{T}}(r) \end{aligned} \quad (2)$$

where  $Z_{\text{T}} (= 3 \text{ au})$  is the charge on the Li nucleus,  $R_{1s}/\sqrt{4\pi}$  is the normalised wave function of the 1s electrons, and  $V_{\text{SR}}^{\text{T}}(r)$  is short range and given by

$$V_{\text{SR}}^{\text{T}}(r) = 2 \int_r^\infty r' \left( \frac{r'}{r} - 1 \right) R_{1s}(r')R_{1s}(r') dr'. \quad (3)$$

The wave function  $R_{1s}$  is taken from the tables of Clementi and Roetti [22] for  $\text{Li}^+$ .

For the interaction between the  $\text{Li}^{2+}(1s)$  projectile and the neutral Li atom we take

$$\begin{aligned} V &= -\frac{Z_{\text{P}}}{|\mathbf{R} - \mathbf{r}|} + Z_{\text{P}}V_{\text{core}}^{\text{T}}(R) + (Z_{\text{P}} - 1)^2V_{\text{pol}}^{\text{core}}(R) \\ &\quad + \frac{1}{4\pi} \int \left[ \frac{1}{|\mathbf{R} + \mathbf{r}' - \mathbf{r}|} - V_{\text{core}}^{\text{T}}(|\mathbf{R} + \mathbf{r}'|) \right] \\ &\quad \times R_{1s}^+(r')R_{1s}^+(r') d\mathbf{r}' \end{aligned} \quad (4)$$

where  $Z_{\text{P}} (= 3 \text{ au})$  is the charge on the  $\text{Li}^{2+}$  nucleus,  $\mathbf{R}$  is the position vector of the  $\text{Li}^{2+}$  nucleus relative to the Li nucleus, and  $R_{1s}^+/\sqrt{4\pi}$  is the hydrogenic wave function for the 1s electron in  $\text{Li}^{2+}$ . The first two terms in (4) represent the interaction of the  $\text{Li}^{2+}$  nucleus with the valence electron of Li and with its

static  $1s^2$  core, while the fourth term gives the corresponding interaction of the frozen  $1s$  electron in  $\text{Li}^{2+}$ . The third term represents the polarization of the  $1s^2$  core by the  $\text{Li}^{2+}$  (1s) projectile. Here we do not take account of the  $1s$  electron and just use the asymptotic charge ( $Z_P - 1$ ), see [15]; for Li core polarization is small.

Using (2) and (4) may be recast as

$$V = -\frac{(Z_P - 1)}{|\mathbf{R} - \mathbf{r}|} + (Z_P - 1)V_{\text{core}}^T(\mathbf{R}) + (Z_P - 1)^2 V_{\text{pol}}^{\text{core}}(\mathbf{R}) - V_P(|\mathbf{R} - \mathbf{r}|) + (Z_T - 2)V_P(\mathbf{R}) + \frac{1}{4\pi} \int [V_{\text{SR}}^T(\mathbf{R}) - V_{\text{SR}}^T(|\mathbf{R} + \mathbf{r}'|)] R_{1s}^+(r') R_{1s}^+(r') d\mathbf{r}' \quad (5)$$

where

$$V_P(X) \equiv \frac{1}{4\pi} \int \left[ \frac{1}{X} - \frac{1}{|\mathbf{X} + \mathbf{r}'|} \right] R_{1s}^+(r') R_{1s}^+(r') d\mathbf{r}'. \quad (6)$$

The first three terms in (5) give the interaction we would have if the  $\text{Li}^{2+}(1s)$  were treated as a bare ion with charge 2 au. The remaining terms give the screening of the  $\text{Li}^{2+}$  nucleus by the frozen  $1s$  electron. The potential  $V_P$  is of short range and is easily calculated. The last term in (5), which is also of short range, requires a little more effort; fortunately it does not depend upon  $\mathbf{r}$  and is a function only of the magnitude of  $\mathbf{R}$ .

Having established the projectile–target interaction potential, according to (5), the theory follows the development of [15], where the reader will find all of the details. To summarize, we introduce a set of orthonormal states  $\psi_\alpha$  for the valence electron in the Li target which diagonalize the atomic Hamiltonian

$$H_A = -\frac{1}{2}\nabla^2 + V_A \quad (7)$$

i.e.

$$\langle \psi_\alpha | H_A | \psi_\beta \rangle = \epsilon_\alpha \delta_{\alpha\beta}. \quad (8)$$

The set of states  $\psi_\alpha$  is so chosen that the lower energy members are good approximations to the valence eigenstates of interest, in particular the  $2s$  and  $2p$  states. The higher members of the set give a discrete representation of the ionized states of the valence electron and are referred to as ‘pseudostates’. In the diagonalization (8) a ‘fictitious’  $1s$  state appears, lying in energy 1.7 au below the  $2s$  ground state; this state is discarded from the set.

The dynamical response of the valence electron under impact is described by the time-dependent wave function  $\Psi$  satisfying

$$(H_A + V)\Psi = i\frac{\partial\Psi}{\partial t} \quad (9)$$

in an impact parameter formalism. We emphasize again that this is an excellent approximation to a full wave treatment at all but the lowest impact energies (see [9]), i.e. it is not to be condemned as a ‘semiclassical’ approximation. The wave function  $\Psi$  is expanded in the set  $\psi_\alpha$  according to

$$\Psi = \sum_\alpha a_\alpha(t, \mathbf{b}) e^{-i\epsilon_\alpha t} \psi_\alpha(\mathbf{r}) \quad (10)$$

where  $\mathbf{b}$  is the impact parameter, i.e.

$$\mathbf{R} = v_0 t \hat{\mathbf{k}} + \mathbf{b} \quad (11)$$

where  $v_0 = v_0 \hat{\mathbf{k}}$  is the incident velocity of the  $\text{Li}^{2+}$  ion relative to the Li target and defines the  $z$ -direction, and

$$\hat{\mathbf{k}} \cdot \mathbf{b} = 0. \quad (12)$$

Substituting (10) into (9) gives the coupled equations

$$i\frac{da_\alpha}{dt} = \sum_\beta e^{i(\epsilon_\alpha - \epsilon_\beta)t} \langle \psi_\alpha | V | \psi_\beta \rangle a_\beta \quad (13)$$

which are solved subject to the boundary conditions

$$a_\alpha(-\infty, \mathbf{b}) = \delta_{\alpha 0} \quad (14)$$

where  $\psi_0$  is the initial state of the valence electron. From the solutions to (13) we can construct an ionization amplitude (see [15] for details)

$$\bar{f}_{\text{ion}}(\kappa, \theta_\kappa, \phi_\kappa - \phi_q, q_t, m_0) \quad (15)$$

where  $m_0$  is the magnetic quantum number of  $\psi_0$  ( $\equiv \psi_{n_0 l_0 m_0}$ ),  $q_t$  is the transverse component (i.e. in the direction perpendicular to  $z$ ) of the momentum transfer  $\mathbf{q}$  (see [15]),  $(q, \theta_q, \phi_q)$  are the polar angles of  $\mathbf{q}$  about the  $z$ -direction, and  $(\kappa, \theta_\kappa, \phi_\kappa)$  are the polar angles of the momentum  $\kappa$  of the ionized electron relative to the Li nucleus. Then the triple differential cross section (TDCS) for observing the ionized electron and the scattered  $\text{Li}^{2+}$  ion in the laboratory, where the Li target is assumed to be initially at rest, is given by

$$\frac{d^3\sigma^L}{dE d\Omega_f d\Omega_\kappa} = \frac{v_f \kappa}{v_0} m_p^2 |\bar{f}_{\text{ion}}|^2 \quad (16)$$

here  $m_p$  is the mass of the projectile and  $v_f$  is the final velocity of the  $\text{Li}^{2+}$  ion after ionization. The TDCS given in (16) is the cross section for the ionized electron being ejected with energy between  $E$  and  $E + dE$  into a solid angle  $d\Omega_\kappa$  while the  $\text{Li}^{2+}$  projectile is scattered into the solid angle  $d\Omega_f$ , all as observed in the laboratory frame of reference. Note that, unlike Ghanbari-Adivi *et al* [8] and Ghorbani *et al* [19], all of our cross sections are given in the laboratory frame of reference [9]. These other authors use the centre-of-mass (relative) coordinate system where the cross section is given by [9]

$$\frac{d^3\sigma}{dE d\Omega_f d\Omega_\kappa} = \frac{v_f \kappa}{v_0} \mu^2 |\bar{f}_{\text{ion}}|^2 \quad (17)$$

$\mu$  being the reduced mass of the  $\text{Li}^{2+}$ —Li system. But, since the projectile and target have essentially the same mass in this case,  $\mu = m_p/2$ , so that

$$\frac{d^3\sigma^L}{dE d\Omega_f d\Omega_\kappa} = 4 \frac{d^3\sigma}{dE d\Omega_f d\Omega_\kappa}. \quad (18)$$

Therefore, in making comparison with their work we have increased their cross sections by a factor of 4. Also of interest here is the double differential cross section (DDCS)

$d^2\sigma/dEdq_t$ , the single differential cross section (SDCS)  $d\sigma/dE$ , the integral cross section  $\sigma_{nlm,n_0l_0m_0}$  for scattering to any final state  $nlm$ , the total ionization cross section  $\sigma_{\text{ion},n_0l_0m_0}$ , and the total cross section  $\sigma_{\text{tot},n_0l_0m_0}$ . Expressions for these are given in [15].

The full coupled state approximation (13) with the full interaction potential (5) we shall label as CP. The coupled equations (13) can also be run in first Born mode by replacing  $a_\beta$  on the right-hand side of (13) by  $\delta_{\beta 0}$ . When this is done using the full potential (5) we shall label the approximation as CPB1. Switching off the contribution of the 1s electron in  $\text{Li}^{2+}(1s)$ , i.e. using only the first three terms in (5), so treating the  $\text{Li}^{2+}(1s)$  as a bare ion of charge  $Z_p - 1 = 2$  au, we can rerun the full coupled state approximation (13) and obtain an approximation which we label as CPBARE. The same approximation run in first Born mode gives us CPBAREB1. From these approximations we can assess how important it is to take explicit account of the 1s electron and how close our results are to the first Born limit. But, furthermore we can also calculate the first Born amplitude for ionization by the bare ion directly from (see [15])

$$\frac{2(Z_p - 1)}{q^2} \langle \psi_{\kappa}^-(\mathbf{r}) | e^{i\mathbf{q}\cdot\mathbf{r}} | \psi_0(\mathbf{r}) \rangle \quad (19)$$

here the ionized wave function  $\psi_{\kappa}^-$  corresponds to an electron with momentum  $\kappa$  scattering off the model potential  $V_A$  with ingoing scattered wave boundary conditions. Since the same potential  $V_A$  is used for the generation of  $\psi_0$  and  $\psi_{\kappa}^-$ , these functions are orthogonal. As a result only the first of the three terms in (5) contribute, which explains the absence of  $V_{\text{core}}^T$  and  $V_{\text{pol}}^{\text{core}}$  from (19). We label this approximation EXBAREB1 since it is an exact first Born approximation, i.e. it does not depend on the choice of a pseudostate basis.

The amplitude (19) is evaluated in partial wave form as described in [15].<sup>3</sup>

### 3. Computational details

The experimental data of Ghanbari-Adivi *et al* [7] cover ejection energies of 2, 10 and 20 eV. For each ejection energy we have used the corresponding 164 state set ( $l = 0$  to 9,  $n = l + 1$  to 21, excluding 1s) constructed in [15] by diagonalizing  $H_A$  in a basis of Laguerre functions,

$$\chi_{klm}(\mathbf{r}) = (\lambda_l r)^l L_{k-1}^{2l+2}(\lambda_l r) e^{-\lambda_l r/2} Y_{lm}(\hat{\mathbf{r}}) \quad (20)$$

with  $k = 1$  to  $(21 - l)$ ,  $l = 0$  to 9. Each set has been constructed so that there is one state  $n = N$  of each angular symmetry ( $lm$ ) with energy exactly equal to that of the ionized electron [15], i.e.

$$\epsilon_{Nlm} = \frac{\kappa^2}{2}. \quad (21)$$

<sup>3</sup> In reference [15], the result is incorrectly quoted. In equation (42) of [15] an overall factor of  $2ZP/q^2$  is missing, while in equation (43) the factor  $(-i)^{l-\lambda} \sqrt{(2\lambda+1)/2} e^{-im} / \pi^2$  should be  $2\sqrt{2(2\lambda+1)} i^{l+\lambda} e^{+im}$ . However, the calculated values for  $f_{\text{ion}}^{B1}$  in reference [15] are correct.

The values of  $\lambda_l$  have been chosen so that the states with  $N = 8$ ,  $N = 11$ , and  $N = 13$  have energies of 2, 10 and 20 eV respectively. All three bases give good energies for the  $n = 2, 3$  and 4 eigenstates of Li. See [15] for details. In calculating the first Born amplitude (19) for ionization of  $\text{Li}(2s)$  and  $\text{Li}(2p)$ , it does not matter from which of the three sets we take the 2s and 2p wave functions, all are equally good for present purposes.

See [15] for further details.

## 4. Results

### 4.1. Triple differential cross sections (TDCS)

Our primary concern in this paper are the TDCS measurements of Ghanbari-Adivi *et al* [8]. These have been made for ionization of  $\text{Li}(2s)$  and  $\text{Li}(2p)$  for ejection energies of 2, 10 and 20 eV and momentum transfers  $q$  of 0.4 au and 1.0 au in each case. Setting up a right-handed Cartesian coordinate system in which the Li target is at the origin and the  $\text{Li}^{2+}$  is incident in the positive  $Z$ -direction and is scattered into the positive half of the  $X - Z$  plane, the measurements observe electron ejection into the  $X - Y$  plane ( $\theta_{\kappa} = \pi/2$ ) as a function of the azimuthal angle  $\phi_{\kappa}$  ( $0 \leq \phi_{\kappa} < 2\pi$ ). The measurements are not absolute but are internormalised for the same Li state. For  $\text{Li}(2p)$  the target is in a mixed combination of magnetic substates:

$$(0.86)\text{Li}(2p_{-1}) + (0.09)\text{Li}(2p_0) + (0.05)\text{Li}(2p_{+1}). \quad (22)$$

It is shown in [15] that

$$\bar{f}_{\text{ion}}(\kappa, \theta_{\kappa}, \phi_{\kappa} - \phi_q, q_t, -m_0) = \bar{f}_{\text{ion}}(\kappa, \theta_{\kappa}, \phi_{\kappa}, \phi_q, q_t, m_0) \quad (23)$$

from which it follows that the TDCS for  $-m_0$  is the mirror image of that for  $+m_0$  in the plane  $\phi_{\kappa} = \phi_q$ . Consequently, for  $m_0 \neq 0$  we have a dichroism, while for  $m_0 = 0$  the TDCS must be symmetric about  $\phi_{\kappa} = \phi_q$ . Equal admixtures of  $-m_0$  and  $+m_0$  would also lead to symmetry about  $\phi_{\kappa} = \phi_q$ , but this is not the case here for  $\text{Li}(2p)$  where the initial state of the target is heavily weighted toward the  $m_0 = -1$  substate (see (22)). As a result, we do not expect to see such symmetry in the  $\text{Li}(2p)$  measurements, but we do expect it in the  $\text{Li}(2s)$  data.

First, let us address the quality of the pseudostate bases used in the present calculations. By comparing CPBAREB1 with EXBAREB1 we get a good indication. For the cases studied here, we find agreement between the two within 1%, except for 20 eV ejection from  $\text{Li}(2p_0)$  at  $q = 0.4$  au; here the difference is about 4% at the peak of the cross section. But then, this is a relatively small cross section, being only about 5% of  $\text{Li}(2p_{\pm 1})$  ionization in the same kinematics. Indeed, we generally find, in all of our approximations, that ionization from  $\text{Li}(2p_0)$  is small compared with that from  $\text{Li}(2p_{\pm 1})$ , for  $q = 0.4$  au, ranging from about 2% to 5% on going from 2 eV ejection to 20 eV ejection, and for  $q = 1.0$  au, varying from 2% to 10% for the same ejection energy range. Consequently, our calculations indicate that the measured cross section (22) is largely ionization from  $\text{Li}(2p_{-1})$ . The agreement between CPBAREB1 and EXBAREB1 suggests that the bases are of very good quality for present purposes.

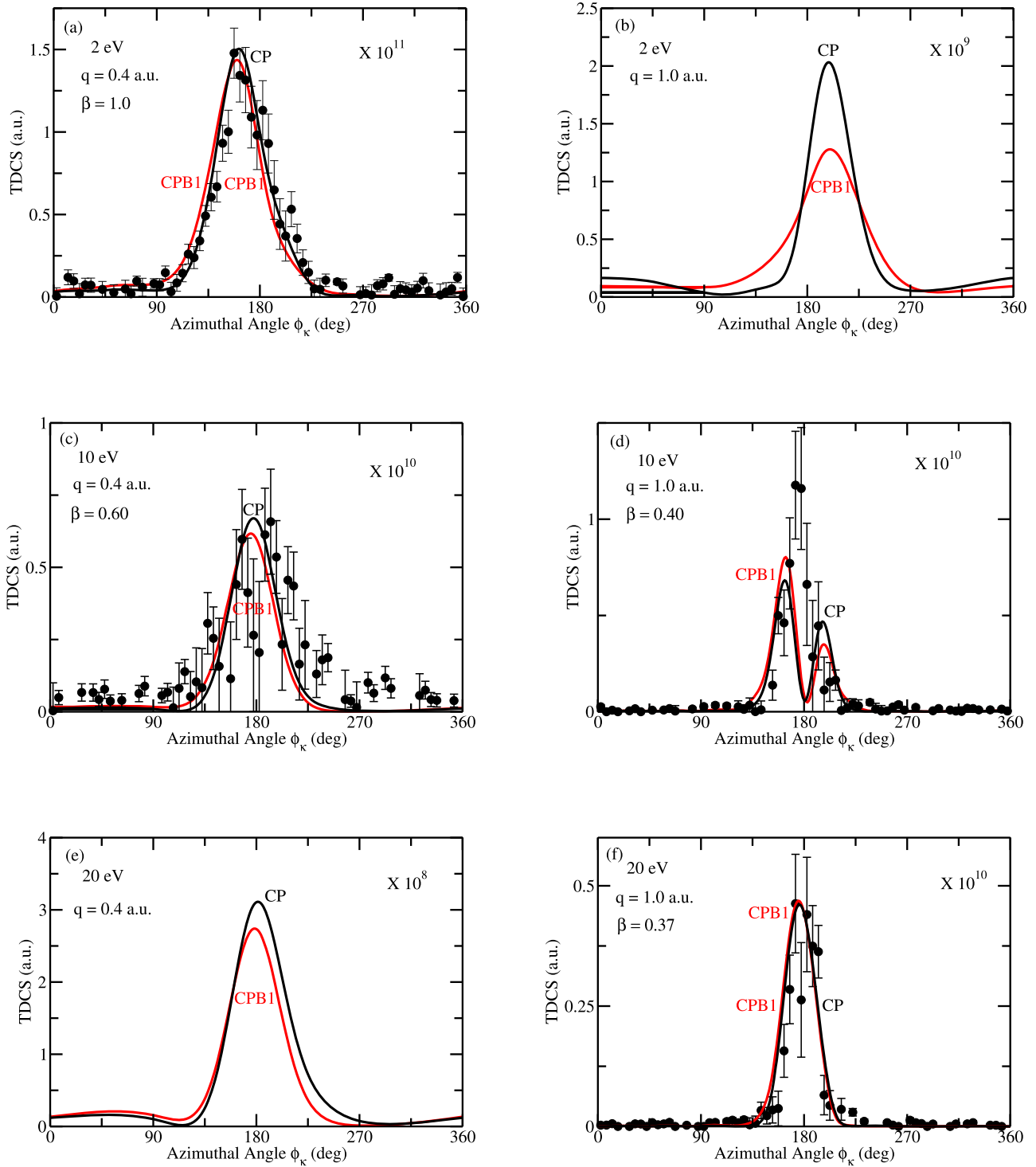


**Figure 2.** TDCS (in the laboratory frame) for 16 MeV  $\text{Li}^{2+}$  impact on  $(0.86)\text{Li}(2p_{-1}) + (0.09)\text{Li}(2p_0) + (0.05)\text{Li}(2p_{+1})$ . The energy of the ejected electron in eV and the momentum transfer  $q$  of the  $\text{Li}^{2+}$  projectile in au are indicated on each panel. Approximations: CP (black curve); CPB1 (red curve). Experimental data from [8] have been normalised as described in text to give best visual fit to CP curve in each case.

Let us now turn to the screening of the  $\text{Li}^{2+}(1s)$  nucleus by the  $1s$  electron. We can see the effect of this screening by comparing CP with CPBARE (or CPB1 with CPBAREB1). Here, in all three cases,  $\text{Li}(2s, 2p_0, 2p_{\pm 1})$ , we see differences in the main peak (the dominant part of the TDCS, see figures 1 and 2) only up to about 6%, the differences usually increasing with  $q$  and with ejection energy. In the geometries studied here,

$1s$  screening is obviously not a significant effect. While we have restricted the dynamics of the  $1s$  electron by freezing it, we find it hard to believe that a more flexible treatment would yield any significant change. We therefore see no evidence that the  $1s$  electron of  $\text{Li}^{2+}$  will explain the discrepancies between the calculations of Ghorbani *et al* [19] and experiment, as these authors have tentatively suggested.



In figure 1 we compare our CP and CPB1 calculations with the experimental data of Ghanbari-Adivi *et al* [8] for ionization of Li(2s). The data have been normalised for best visual fit to the CP curve for 2 eV ejection at  $q = 0.4$  au. This should fix the normalisation of the Li(2s) measurements in all the other cases. However, as Ghanbari-Adivi *et al* [8] also find in comparison with their 3DW-EIS theory, this results in experimental cross sections which are too high in the other cases. We have therefore applied a further normalisation by a factor  $\beta$  to give the best visual fit of the other measurements to our CP results; this factor is indicated on each of the figures. The changes in normalisation are substantial.

At 2 eV ejection, the TDCS decreases by an order of magnitude on going from  $q = 0.4$  au to  $q = 1.0$  au (figures 1(a) and (b)), but the reverse is true for 10 and 20 eV ejection (figures 1(c) through (f)). Where the cross section is largest (2 eV,  $q = 0.4$  au; 10 and 20 eV,  $q = 1.0$  au) there is generally good agreement between experiment and the CP values. But it is also clear from the agreement between CP and CPB1 that, in these cases, the cross section is largely first Born. For the other situations (figures 1(b), (c), (e)) where the cross section is an order of magnitude smaller, CP and CPB1 differ noticeably, but yet not that much. Here experiment is more scattered but still in fair accord with the CP results. In particular, for 2 eV ejection at  $q = 1.0$  au (figure 1(b)) the experimental data agree well with the width of the CP peak.

Figure 2 compares our CP and CPB1 calculations with the experimental data of Ghanbari-Adivi *et al* [8] for Li(2p) in the combination (22) [8]. The data have been normalised for best visual fit to the CP results at 2 eV ejection energy and  $q = 0.4$  au (figure 2(a)). As in the Li(2s) case, and consistent with the 3DW-EIS calculations of Ghanbari-Adivi *et al* [8], this results in experimental cross sections which are much too high compared with theory in the other kinematics. As with Li(2s), we therefore introduce a further normalisation factor  $\beta$  to give best visual fit in the other cases.

For 2 eV ejection and  $q = 0.4$  au (figure 2(a)) we see good agreement with the experimental data, but we also notice that the difference between CP and CPB1 is small, indicating that we are again close to the first Born limit. Nevertheless, it is clear that the experimental data have a preference for the CP cross section, rather than CPB1. The results show a single peak located near  $\phi_\kappa = 162^\circ$ . In the absence of the  $2p_{\pm 1}$  dichroism, this would have been placed symmetrically about  $\phi_\kappa = 180^\circ$ , as we have seen for the Li(2s) results (figure 1). As  $q$  is increased from 0.4 au to 1.0 au, figure 2(b) shows that the TDCS falls by two orders of magnitude and now displays a substantial difference between CP and CPB1, although both again indicate a single peak near  $\phi_\kappa = 200^\circ$ , i.e. on the opposite side of  $\phi_\kappa = 180^\circ$  from  $q = 0.4$  au. Unfortunately, there are no experimental data for this geometry.

Figures 2(c) and (d) show an interesting situation for 10 eV ejection. At  $q = 0.4$  au (figure 2(c)) there is close agreement between the CP and CPB1 approximations with a single peak near  $\phi_\kappa = 178^\circ$  for CP and  $\phi_\kappa = 175^\circ$  for CPB1. The cross section is an order of magnitude smaller than for 2 eV ejection at the same  $q$  (figure 2(a)). The experimental

data are somewhat scattered but consistent with the theoretical results (except in respect of normalisation,  $\beta = 0.60$ ). When  $q$  is increased to 1.0 au (figure 2(d)), the overall magnitude of the cross section remains unchanged and CP and CPB1 stay in relatively close agreement. But now we see a split peak, the dominant peak appearing near  $\phi_\kappa = 164^\circ$ , the less dominant near  $\phi_\kappa = 197^\circ$ , with a minimum between the two near  $\phi_\kappa = 182^\circ$ . The CP and CPB1 approximations differ essentially in the ratio of the two peaks, the CP approximation giving a smaller ratio 1.46 of the large peak to the small peak compared with the greater ratio 2.26 of the CPB1 approximation. The experimental data are insufficiently refined to distinguish such a two-peak structure and only in modest accord with theory.

For 20 eV ejection (figures 2(e) and (f)) we again see a single peak at both  $q$  values. The  $q = 0.4$  au cross section is almost two (three) orders of magnitude smaller than for 10 eV (2 eV) ejection. In this case the peak in CP and CPB1 is near to  $\phi_\kappa = 180^\circ$ . While the CP and CPB1 approximations are close, there is still a clear difference between them. There are no experimental data for this case. When  $q$  is increased to 1.0 au (figure 2(f)) the cross section grows by an order of magnitude, the peak moves to near  $\phi_\kappa = 176^\circ$ , and the CP and CPB1 approximations become very close. The experimental data are consistent with theory but the error bars are large.

How do our results compare with the original 3DW-EIS calculations of Ghanbari-Adivi *et al* [8]? We show this comparison for Li(2s) in figure 3 and for Li(2p) in figure 4. Although there are some differences in detail, we see from figure 3 that the Li(2s) results are very comparable.

The same is true for Li(2p), except for 20 eV ejection at  $q = 0.4$  au (figure 4(e)). Whereas CP predicts a single peak, 3DW-EIS displays a peak with pronounced shoulders on each side. However, the central peak heights of the 3DW-EIS and CP approximations are in very good accord. In figure 4(e) we also show the CDW-EIS calculation of Ghorbani *et al* [19]. In contrast to 3DW-EIS, this approximation is in very good agreement with CP. Yet, when we compare CDW-EIS with CP for 2 eV ejection and  $q = 1.0$  au (figure 4(b)) there is complete discord, with CP predicting a single peak but CDW-EIS giving a pronounced two peak structure. Now, paradoxically, 3DW-EIS is quite close to CP. It is unclear how these pronounced differences arise, but the two cases, 2 eV ejection with  $q = 1.0$  au and 20 eV ejection with  $q = 0.4$  au, are cases in which the TDCS is relatively small (see figure 2), in fact so small that experiment was unable to measure them. In such a situation it is to be expected that the TDCS will be much more sensitive to the details of the approximation. However, we would point out that CP is the one constant factor here, agreeing well with one of the other approximation in each case.

#### 4.2. Double differential cross section (DDCS) $d^2\sigma/dEdq_t$

In figures 5 and 6 we show the DDCS  $d^2\sigma/dEdq_t$  for ionization of Li(2s) and Li( $2p_{0,\pm 1}$ ) for the three ejection energies 2, 10 and 20 eV. Unlike figure 1 which refers to particular kinematics of the TDCS,  $d^2\sigma/dEdq_t$  is a sum over all outgoing directions of the ionized electron and all azimuthal directions

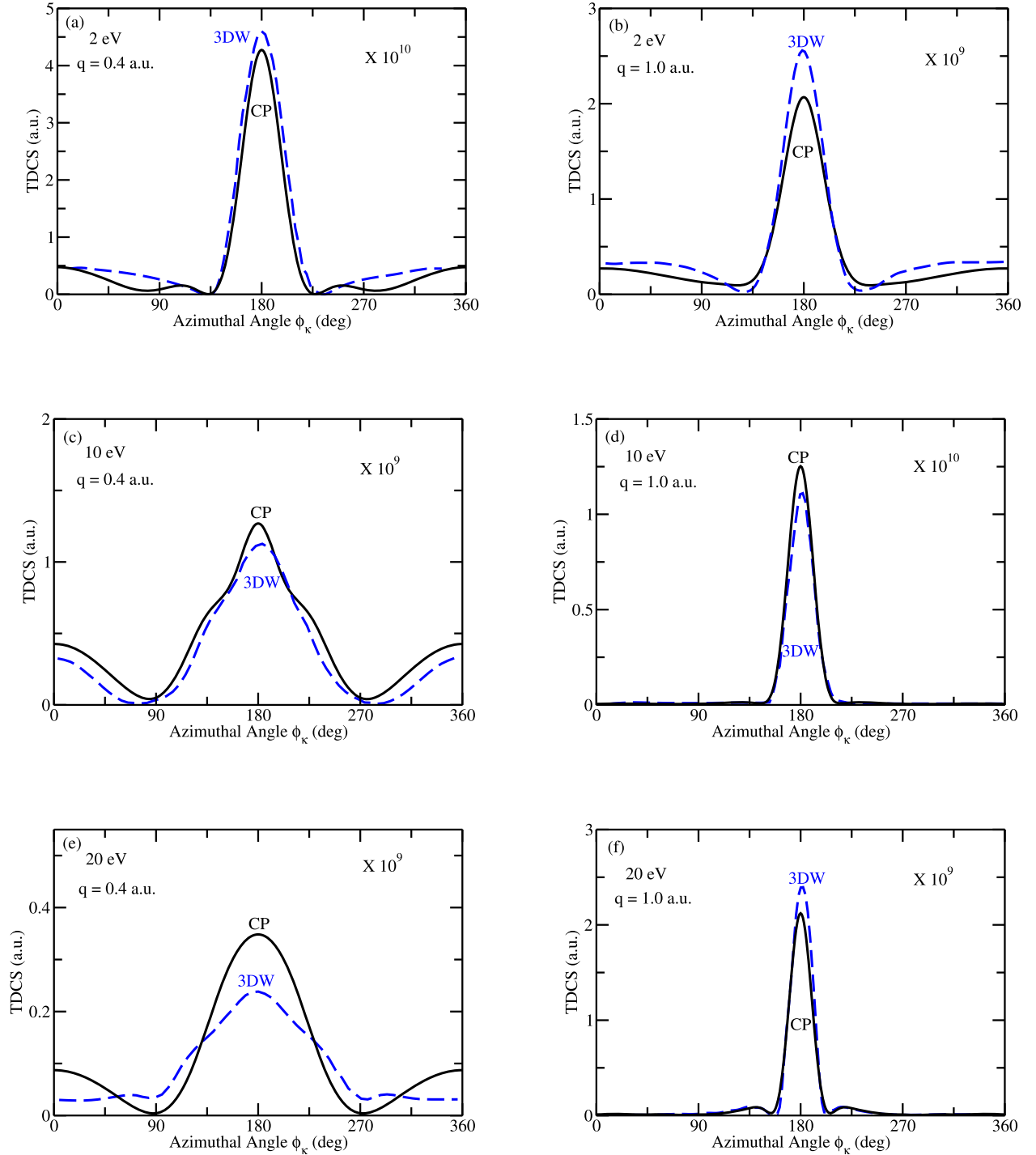


**Figure 3.** Comparison of the present CP approximation with the 3DW-EIS approximation of Ghanbari-Adivi *et al* [8] for 16 MeV  $\text{Li}^{2+}$  impact on  $\text{Li}(2s)$ . The TDCS is given in the laboratory frame of reference. The energy of the ejected electron in eV and the momentum transfer  $q$  of the  $\text{Li}^{2+}$  projectile in au are indicated on each panel. CP, black continuous curve; 3DW-EIS, blue dashed curve (indicated as 3DW in figures).

of the momentum transfer:

$$\frac{d^2\sigma}{dEdq_t} = \frac{q_t}{k_0 k_f} \int_0^{2\pi} \frac{d^2\sigma}{dEf d\Omega_f} d\phi_q \quad (24)$$

where

$$\frac{d^2\sigma}{dEd\Omega_f} = \int \frac{d^3\sigma}{dEd\Omega_f d\Omega_\kappa} d\Omega_\kappa \quad (25)$$

and  $k_0 = \mu v_0$ ,  $k_f = \mu v_f$ .

We have seen that our pseudostate bases are of sufficiently good quality to represent the TDCSs of figures 1 and 2. But, are they good enough for calculating the DDCS which extends over a larger range of kinematics. Again, we can get an insight by comparing CPBAREB1 with EXBAREB1. For the range of  $q_t$  shown in figures 5 and 6 we find excellent agreement between the two, except for  $\text{Li}(2p_{0,\pm 1})$  at 20 eV ejection. For  $\text{Li}(2p_0)$  the EXBAREB1 cross section can be up to 10% larger

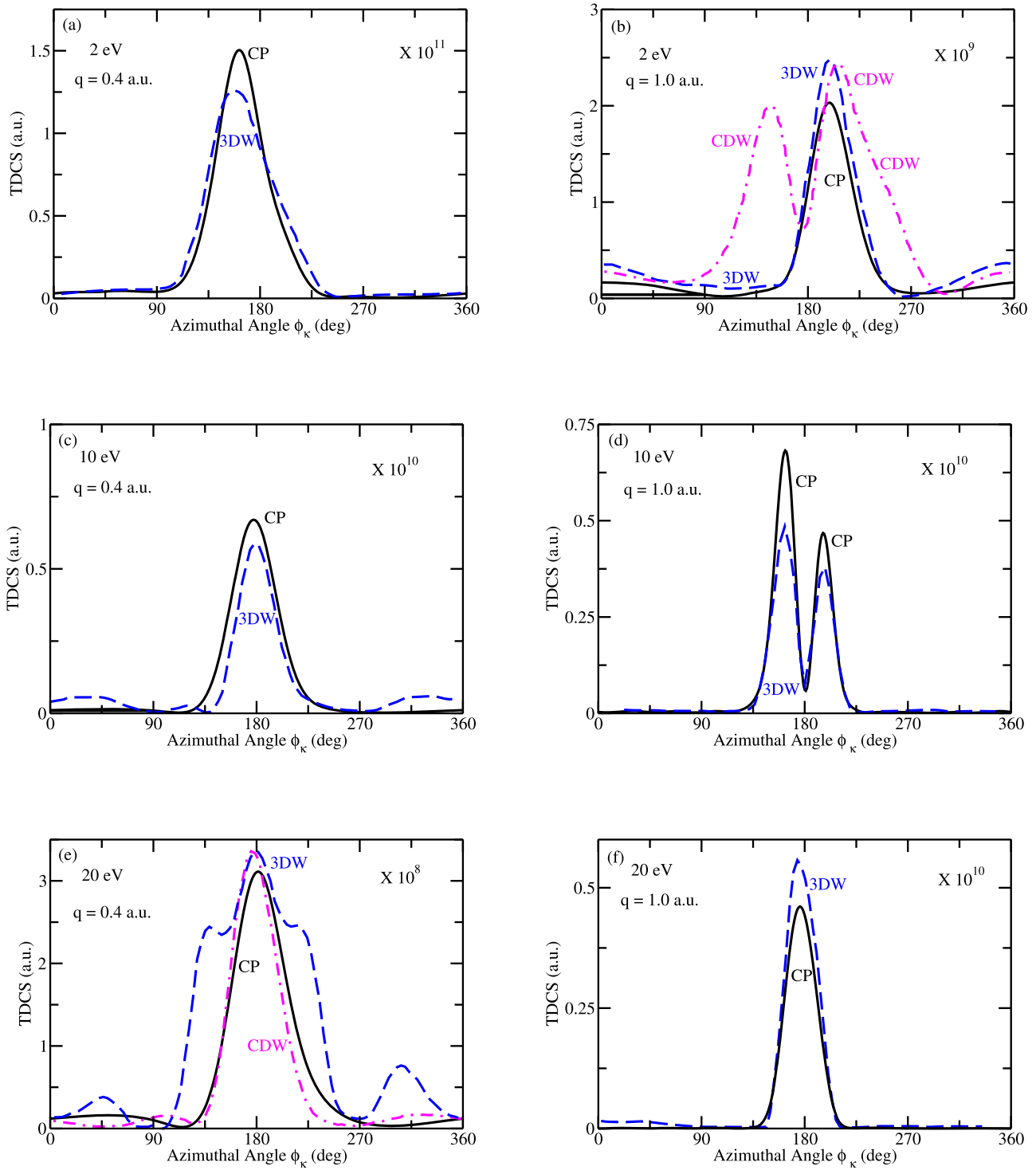


**Figure 4.** Comparison of the present CP approximation with the approximations of Ghanbari-Adivi *et al* [8] (3DW-EIS) and Ghorbani *et al* [19] (CDW-EIS (full prior form)) for 16 MeV  $\text{Li}^{2+}$  impact on  $(0.86)\text{Li}(2p_{-1}) + (0.09)\text{Li}(2p_0) + (0.05)\text{Li}(2p_{+1})$ . The TDCS is given in the laboratory frame of reference. The energy of the ejected electron in eV and the momentum transfer  $q$  of the  $\text{Li}^{2+}$  projectile in a.u. are indicated on each panel. CP, black continuous curve; 3DW-EIS, blue dashed curve (indicated as 3DW in figures); CDW-EIS, magenta dash-dot curve (indicated as CDW in figures).

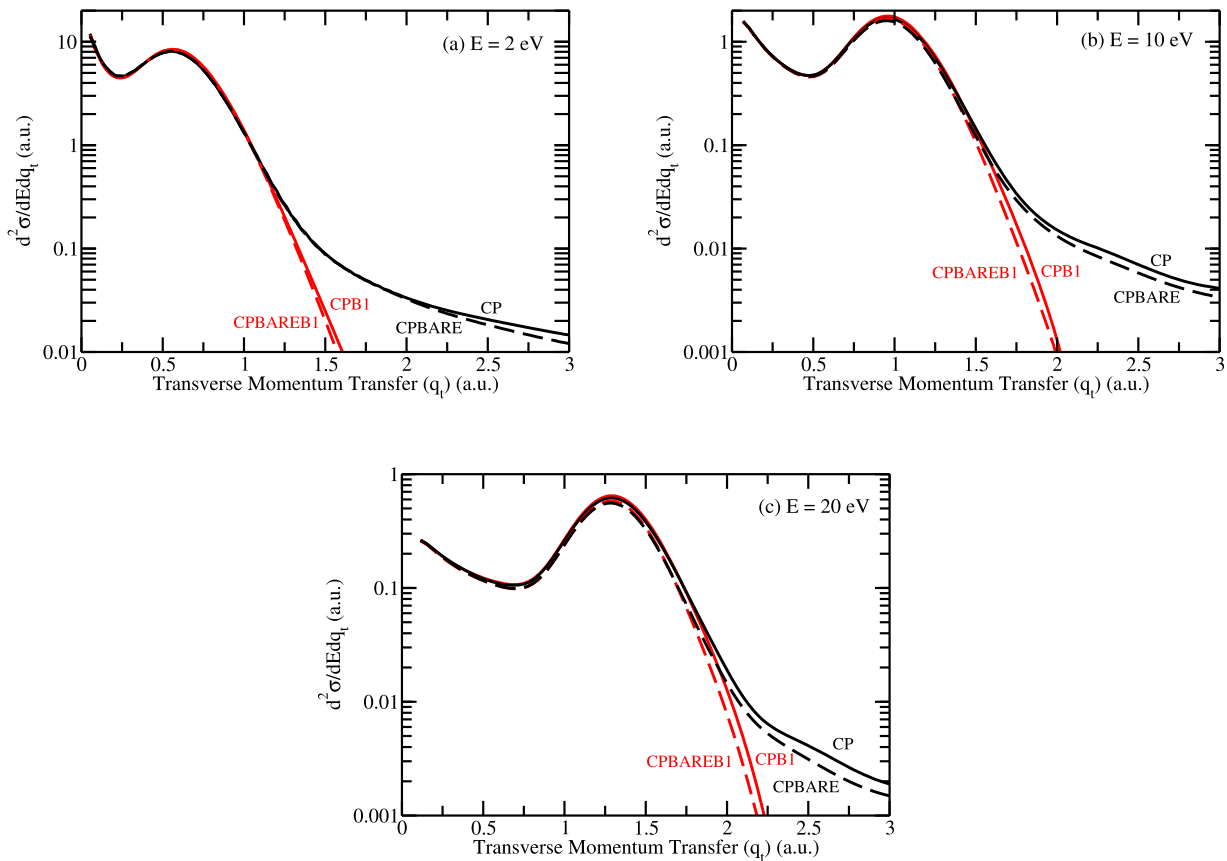


**Figure 5.** Cross section  $d^2\sigma/dEdq_t$  for  $\text{Li}^{2+}$  impact ionization of  $\text{Li}(2s)$  at 16 MeV and at ejected electron energies  $E$  of 2, 10 and 20 eV. Approximations: CP, solid black curve; CPBARE, dashed black curve; CPB1, solid red curve; CPBAREB1, dashed red curve.

than CPBAREB1 near the peak, and for  $\text{Li}(2p_{\pm 1})$  up to 5% larger, but with very good agreement elsewhere. The difference can be traced primarily to the number of partial waves  $l$  included in the pseudostate set. This is restricted to  $l \leq 9$  (see section 3). In the EXBAREB1 approximation (19) we can add as many partial waves as necessary for convergence, see (?). The implication is that the pseudostate basis should go a little higher in angular momenta for these cases.<sup>4</sup> This observation was also made in [15] for  $\text{O}^{8+} + \text{Li}(2p)$  ionization at 1.5 MeV/amu. See [15] for further discussion.

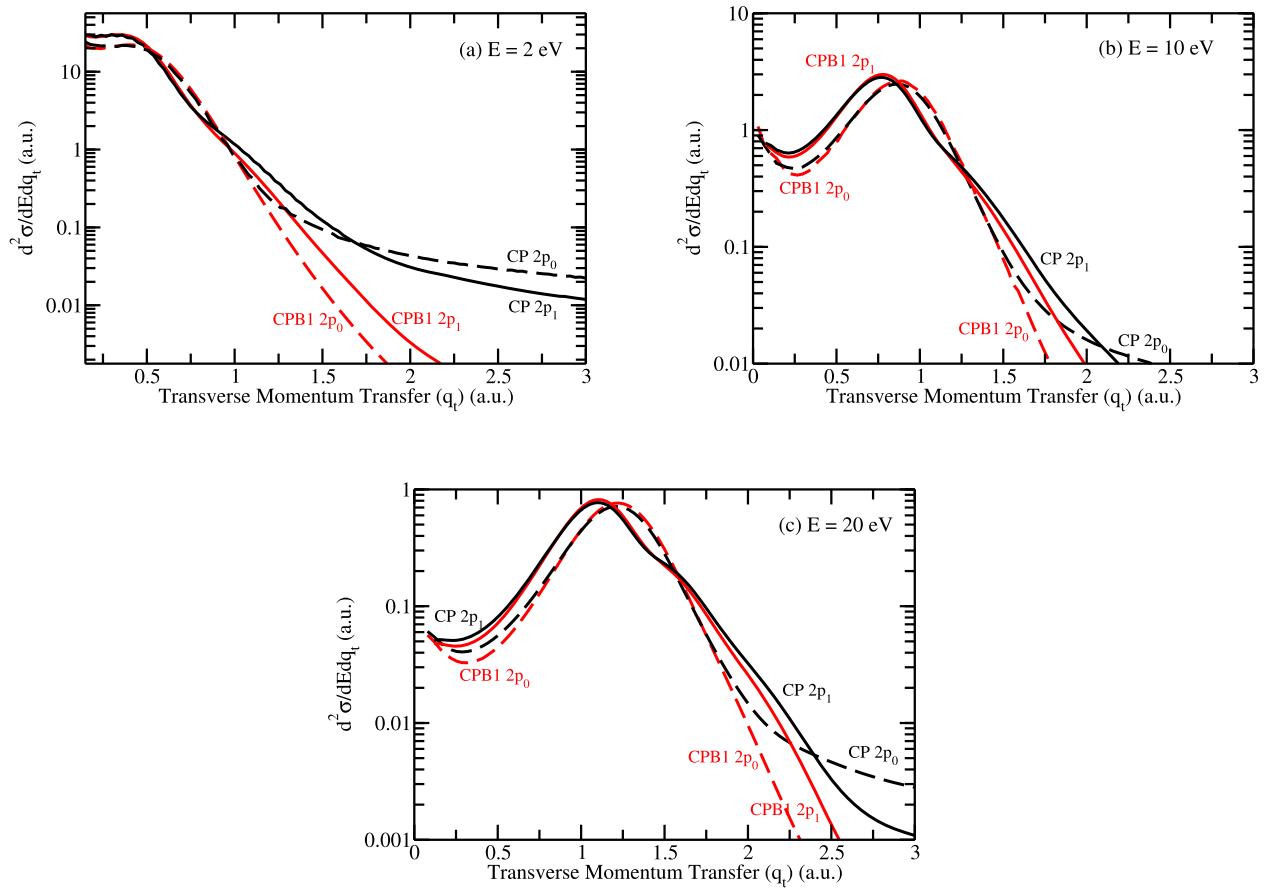
Now let us look at specific cases. Figure 5 shows  $d^2\sigma/dEdq_t$  for ionization of  $\text{Li}(2s)$ . Here we show the CP, CPBARE, CPB1 and CPBAREB1 approximations. At low  $q_t$  there is convergence between CP and CPB1 and between CPBARE and CPBAREB1. This reflects proximity to the first Born limit, which we have also seen in figure 1. At large  $q_t$  the first Born cross sections start to fall very rapidly below their full counterparts, CP and CPBARE. This is because the first Born approximations lack the interaction between the  $\text{Li}^{2+}$  and Li nuclei (see (19)) which is necessary to sustain the cross section at large  $q_t$ . This is clearly shown in the theoretical calculations of [9–13, 15] and in the experimental data quoted in [15].

Figure 5 also shows the effect of shielding by the 1s electron in the  $\text{Li}^{2+}(1s)$  (compare CP and CPBARE, CPB1 and CPBAREB1). As with the TDCS, discussed in section 4.1, shielding effects are small at low  $q_t$  but more significant at large  $q_t$  (where the cross section is anyway relatively small) and with increasing ejection energy  $E = \kappa^2/2$ . This makes sense in that large  $q_t$  collisions involve a close encounter between the two nuclei and large ejection energies require a hard (and therefore penetrating) collision between the projectile and the ionized electron. It is noteworthy that the full cross sections lie above the bare cross sections. In the full cross sections the  $\text{Li}^{2+}(1s)$  effective nuclear charge varies from 3 au close in, to 2 au asymptotically, as a result of the screening, whereas, in the bare cross sections the  $\text{Li}^{2+}(1s)$  effective nuclear charge is constant at 2 au at all distances.

In figure 6 we show  $d^2\sigma/dEdq_t$  for ionization of  $\text{Li}(2p_0)$  and  $\text{Li}(2p_{\pm 1})$ .<sup>5</sup> In the interests of clarity we do not show the bare cross sections CPBARE and CPBAREB1; suffice it to say that the differences between CP and CPBARE and between CPB1 and CPBAREB1 are comparable to those seen in figure 5. For both  $\text{Li}(2p_0)$  and  $\text{Li}(2p_{\pm 1})$  we see convergence to the first Born limit CPB1 at small  $q_t$  for 2 eV ejection, and in the peak region for 10 and 20 eV ejection; in these latter two cases CPB1 falls below CP on further reduction of  $q_t$ . At

<sup>4</sup> But this would lead to a large increase in the magnitude of the calculation, which, for present purposes, would not be worthwhile.

<sup>5</sup>  $d^2\sigma/dEdq_t$  for  $\text{Li}(2p+1)$  is the same as that for  $\text{Li}(2p-1)$ , see [15].



**Figure 6.** Cross section  $d^2\sigma/dEdq_t$  for  $\text{Li}^{2+}$  impact ionization of  $\text{Li}(2p_{0,\pm 1})$  at 16 MeV and at ejected electron energies  $E$  of 2, 10 and 20 eV. Solid curves  $\text{Li}(2p_{\pm 1})$ : CP, black; CPB1, red. Dashed curves  $\text{Li}(2p_0)$ : CP, black; CPB1, red.

large  $q_t$  we again see CPB1 falling well below CP as a result of the Born approximation lacking the nucleus–nucleus interaction. The cross sections for  $\text{Li}(2p_0)$  peak at larger  $q_t$  than those for  $\text{Li}(2p_{\pm 1})$ , there lying above the  $\text{Li}(2p_{\pm 1})$  cross section, but lying below the latter at smaller and larger  $q_t$ , except that at large  $q_t$  the CP cross section for  $\text{Li}(2p_0)$  eventually exceeds that for  $\text{Li}(2p_{\pm 1})$ . We notice also a shoulder in the vicinity of  $q_t = 1.0$  au (1.5 au) (1.75 au) for 2 eV (10 eV) (20 eV) ejection. Such a shoulder was observed in the calculations of [15] for  $\text{O}^{8+}$  impact on  $\text{Li}(2p_{\pm 1})$  at 1.5 MeV/amu and was also noticeable in the corresponding experimental data.

#### 4.3. Single differential cross section (SDCS) $d\sigma/dE$

In figure 7 we show  $d\sigma/dE$  for initial states  $\text{Li}(2s)$ ,  $\text{Li}(2p_0)$  and  $\text{Li}(2p_{\pm 1})$  in the CP and CPB1 approximations (from best estimates from our three pseudostate bases, see section 3). The  $\text{Li}(2p_0)$  and  $\text{Li}(2p_{\pm 1})$  cross sections are very similar and almost an order of magnitude larger than  $\text{Li}(2s)$  at low energies (less than about 1 eV). With increasing ejection energy the  $\text{Li}(2s)$  cross section eventually crosses over the  $\text{Li}(2p_{0,\pm 1})$  curves, becoming the largest just beyond 10 eV.

We have also calculated  $d\sigma/dE$  in the CPBARE and CPBAREB1 approximations (not shown) and find minor differences from CP and CPB1 up to a few eV of the ejection energy  $E$ . In this energy range screening by the 1s electron

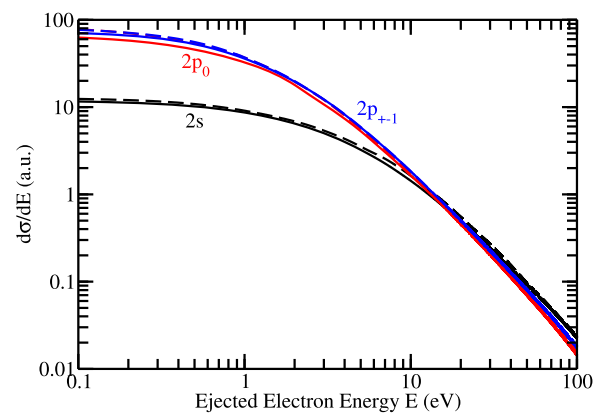


**Figure 7.** Cross section  $d\sigma/dE$  for  $\text{Li}^{2+}(1s)$  impact on  $\text{Li}(2s)$  (black curves),  $\text{Li}(2p_0)$  (red curves) and  $\text{Li}(2p_{\pm 1})$  (blue curves) at 16 MeV. Solid curves, CP approximation; dashed curves, CPB1 approximation.

in the  $\text{Li}^{2+}(1s)$  is clearly not so important. However, asymptotically in  $E$  the BARE cross sections lie below the CP and CPB1 results. The reason has already been given in discussing figure 5. For large energy ejection a hard close collision between the projectile and the ionized electron is required. This interaction is stronger when screening is taken into account as the effective nuclear charge of the projectile

then varies between 2 and 3 au, which is to be compared with the fixed nuclear charge of 2 au in the BARE approximations.

#### 4.4. Integrated cross sections

In table 1 we show the calculated integral cross sections for  $\text{Li}^{2+} + \text{Li}(2s, 2p_{0,\pm 1})$  at 16 MeV in the CP, CPB1 and CPBARE approximations. These include transitions to the  $n = 2, 3$  and 4 states, an aggregate of discrete transitions to  $n \geq 5$  (labeled ‘other discrete’), the ionization cross section and the total cross section. The results presented are the best estimates from our three pseudostate bases (for  $E = 2, 10$  and 20 eV, see section 3). From comparison of the different bases we estimate that our cross sections for the initial states  $\text{Li}(2s)$  and  $\text{Li}(2p_{\pm 1})$  are accurate to about 2%, except for  $n = 4$  and other discrete transitions which have an accuracy of about 5%. For  $\text{Li}(2p_0)$ , things seem to be a little more sensitive, with an estimated accuracy of 3% except for the  $n = 4$  and other discrete transitions which now have an accuracy of 10%, and for the transition  $\text{Li}(2p_0) \rightarrow \text{Li}(2s)$  which also has an accuracy of about 10%.

From the table we see that there is not a great deal of difference between the three approximations for the  $n = 4$ , other discrete, and ionization transitions. Nor is there between the CP and CPBARE approximations except for the resonance transition  $\text{Li}(2s) \rightarrow \text{Li}(2p)$ , only here does the screening of the 1s electron in  $\text{Li}^{2+}(1s)$  seem to have a substantial effect. The first Born CPB1 approximation is not greatly at variance with CP, and often very close, as we might expect at such a high impact energy.

For  $\text{Li}(2s)$  the dominant transition is, as expected, to  $\text{Li}(2p)$ . For  $\text{Li}(2p_{0,\pm 1})$  the dominant transition is to  $\text{Li}(3d)$  with  $\text{Li}(2s)$  being close behind for  $\text{Li}(2p_{\pm 1})$ . Again, this is as expected as these are optically allowed transitions. Ionization is only about 8% of the  $\text{Li}(2s)$  total cross section and less than about 15% of the  $\text{Li}(2p_{0,\pm 1})$  totals.

## 5. Conclusions

We have applied the powerful coupled pseudostate method [9–18] to  $\text{Li}^{2+} + \text{Li}(2s, 2p_{0,\pm 1})$  collisions at 16 MeV with emphasis on studying the TDCS cross section measurements of Ghanbari-Adivi *et al* [8] in the azimuthal plane. These measurements have been made for ejected electron energies of 2, 10 and 20 eV and for momentum transfers  $q = 0.4$  and 1.0 au. Except for normalisation, the agreement with the experimental data is generally quite good. But, where the agreement is best (where the cross sections are largest) we find that the cross section is very much first Born, i.e. it is no test of higher order approximations. While the relative normalisation of the experimental data is tentative, its trends are totally at variance with our calculations. In this we are in complete accord with the 3DW-EIS calculations of Ghanbari-Adivi *et al* [8]. Indeed, the 3DW-EIS calculations are generally in quite good agreement with our pseudostate results except for the case of 20 eV ejection from  $\text{Li}(2p)$  at momentum transfer  $q = 0.4$  au (figure 4(e)). Here, 3DW-EIS exhibits a pronounced shoulder structure which is absent from our single-peak cross section.

However, in this case the pseudostate cross section is in very good agreement with the CDW-EIS approximation of Ghorbani *et al* [19]. But for 2 eV ejection from  $\text{Li}(2p)$  at  $q = 1.0$  au (figure 4(b)) the situation is completely reversed, with now pronounced disagreement with CDW-EIS but good agreement with 3DW-EIS ! The one constant factor in these two cases is the pseudostate result which is supported by one of the two other approximations. In these two exceptional cases the cross section is relatively small and, unfortunately, there are no experimental data (presumably because the cross section is so small) to test the theoretical results. Where cross sections are relatively small it is usually a more sensitive test of the accuracy of the approximation and we must expect to see differences, but differences that are not important on the overall larger scale.

In the 3DW-EIS and CDW-EIS calculations of Ghanbari-Adivi *et al* [8] and Ghorbani *et al* [19] the  $\text{Li}^{2+}$  has been treated as a bare ion with a nuclear charge of 2 au. In our work we have made explicit allowance for screening by the remaining electron, which we assume to be frozen in the 1s state. This means that the effective nuclear charge of our projectile varies from 2 au at large distance to 3 au close in to the  $\text{Li}^{2+}$  nucleus. As far as the TDCS measurements are concerned we find little effect of the screening (less than about 6% at most), which refutes the conjecture of Ghorbani *et al* [19] that some of the differences they see between their CDW-EIS calculations and experiment could be due to the neglect of the 1s electron in the  $\text{Li}^{2+}$ .

Where we do see noticeable effects of the screening is in large momentum transfer collisions and where the ionized electron has a large ejection energy. Both of these situations require a hard close collision between the projectile nucleus and the ionized electron and so the ionized electron senses the variation in the effective nuclear charge from 2 au to 3 au. This is seen in our large  $q_t$  and large  $E$  results for the DDCS  $d^2\sigma/dEdq_t$  (figure 5) and in the SDCS  $d\sigma/dE$  at large ejected energy  $E$  (see section 4.3). Here proper account of the screening leads to larger cross sections compared with a bare charge of 2 au since the effective screened charge is on average greater than 2 au.

In the DDCS results for  $d^2\sigma/dEdq_t$  (figures 5 and 6) we again see the importance of the NN interaction at large momentum transfers. Here the first Born cross sections, which lack the NN interaction, become orders of magnitude smaller than their full counterparts at large  $q_t$ . By contrast, at smaller  $q_t$ , where the NN interaction is no longer dominant, there is convergence between the two. A point of interest here is that the  $\text{Li}(2p_{0,\pm 1})$  cross sections are almost an order of magnitude larger at small  $q_t$  than that for  $\text{Li}(2s)$ , reflecting the lower binding energy of the 2p electron compared with 2s.

As shown in the appendix of [15], the NN interaction does not contribute to the SDCS  $d\sigma/dE$ . Here we find reasonable agreement between the first Born and full cross sections (figure 7).

Finally, we get to a major strength of the coupled pseudostate approximation, namely that it gives a complete and internally consistent picture of all the main processes. This is seen in table 1 where, as a spin-off from our ionization

calculations, we get results for the discrete transitions up to  $n = 4$  and we see that ionization is a relatively minor process, amounting to only 8% and 15% respectively of the total cross sections for  $\text{Li}(2s)$  and  $\text{Li}(2p_{0,\pm 1})$ .

It is clear from the results presented here that the TDCS measurements of Ghanbari-Adivi *et al* [8] have probed only the first Born regime. It would be interesting to see such measurements at a much lower, but not too low, impact energy where higher order effects may be rigorously tested. Since the pseudostate theory is able to give a complete picture of all the lower order differential cross sections, it would also be useful to have results for these as well in order to test the internal consistency both of theory and experiment.

## Acknowledgments

We are indebted to Michael Schulz and Daniel Fischer for discussions on the data of Ghanbari-Adivi *et al* [8] and for providing tabulations of the same.

## ORCID iDs

H R J Walters  <https://orcid.org/0000-0002-9665-6068>

## References

- [1] Dörner R, Mergel V, Jagutzki O, Spielberger L, Ullrich J, Moshhammer R and Schmidt-Böking H 2000 *Phys. Rep.* **330** 192
- [2] Ullrich J, Moshhammer R, Dorn A, Dörner R, Schmidt L and Schmidt-Böking H 2003 *Rep. Prog. Phys.* **66** 1463
- [3] Fischer D *et al* 2012 *Phys. Rev. Lett.* **109** 113202
- [4] Hubele R *et al* 2015 *Rev. Sci. Instrum.* **86** 033105
- [5] LaForge A C *et al* 2013 *J. Phys. B* **46** 031001
- [6] Hubele R *et al* 2013 *Phys. Rev. Lett.* **110** 133201
- [7] Ghanbari-Adivi E, Fischer D, Ferreira N, Goullon J, Hubele R, LaForge A, Schulz M and Madison D 2016 *Phys. Rev. A* **94** 022715
- [8] Ghanbari-Adivi E, Fischer D, Ferreira N, Goullon J, Hubele R, LaForge A, Schulz M and Madison D 2017 *J. Phys. B: At. Mol. Opt. Phys.* **50** 215202
- [9] McGovern M, Assafrão D, Mohallem J R, Whelan C T and Walters H R J 2009 *Phys. Rev. A* **79** 042707
- [10] McGovern M, Assafrão D, Mohallem J R, Whelan C T and Walters H R J 2009 *J. Phys.: Conf. Ser.* **194** 012042
- [11] McGovern M, Assafrão D, Mohallem J R, Whelan C T and Walters H R J 2010 *Phys. Rev. A* **81** 032708
- [12] McGovern M, Assafrão D, Mohallem J R, Whelan C T and Walters H R J 2010 *J. Phys.: Conf. Ser.* **212** 012029
- [13] McGovern M, Walters H R J and Whelan C T 2013 *Fragmentation Processes* ed C T Whelan (Cambridge: Cambridge University Press) p 155
- [14] McGovern M, Assafrão D, Mohallem J R, Whelan C T and Walters H R J 2010 *Phys. Rev. A* **81** 042704
- [15] Walters H R J and Whelan C T 2014 *Phys. Rev. A* **89** 032709
- [16] Walters H R J and Whelan C T 2015 *Phys. Rev. A* **92** 062712
- [17] McGovern M, Whelan C T and Walters H R J 2010 *Phys. Rev. A* **82** 032702
- [18] Walters H R J and Whelan C T 2012 *Phys. Rev. A* **85** 062701
- [19] Ghorbani O, Ghanbari-Adivi E and Ciappina M F 2018 *J. Phys. B: At. Mol. Opt. Phys.* **51** 095202
- [20] Crothers D S F 1982 *J. Phys. B: At. Mol. Phys.* **15** 2061
- [21] Crothers D S F and McCann J F 1983 *J. Phys. B: At. Mol. Phys.* **16** 3229
- [22] Clementi E and Roetti C 1974 *At. Data Nucl. Data Tables* **14** 177
- [23] Campeanu R I, Walters H R J and Whelan C T 2018 *Phys. Rev. A* **97** 062702
- [24] Stein M 1993 *J. Phys. B: At. Mol. Opt. Phys.* **26** 2087